SIN-CHN SCIENTIFIC PRESS PTE.LTD.

Molecular & Cellular Biomechanics 2024, 21, 111.
https://doi.org/10.62617/mcb.v21.111

Article

Molecular dynamics insight into drug-loading capacity of dodecylphosphocholine aggregate for doxorubicin

Qijiang Shu[1,2,3,*], Qin Lv[4], Zhi Dong[4], Wenping Wang[4], Zedong Lin[5], Pengru Huang[6,*]

[1] Institute of Information, Yunnan University of Chinese Medicine, Kunming 650500, China
[2] Yunnan Key Laboratory of Southern Medicinal Utilization, Yunnan University of Chinese Medicine, Kunming 650500, China
[3] Yunnan Traditional Chinese Medicine Prevention and Treatment Engineering Research Center, Yunnan University of Chinese Medicine, Kunming, 650500, China
[4] College of Chinese Materia Medica, Yunnan University of Chinese Medicine, Kunming 650500, China
[5] Guangdong Provincial Key Lab of Nano-Micro Materials Research, School of Advanced Materials, Shenzhen Graduate School, Peking University, Shenzhen 518055, China
[6] Guangxi Key Laboratory of Information Materials and Guangxi Collaborative Innovation Center of Structure and Property for New Energy and Materials, School of Material Science & Engineering, Guilin University of Electronic Technology, Guilin 541004, China
*** Corresponding authors:** Qijiang Shu, 14787485422@163.com; Pengru Huang, pengruhuang@guet.edu.cn

CITATION

Shu Q, Lv Q, Dong Z, et al. Molecular dynamics insight into drug-loading capacity of dodecylphosphocholine aggregate for doxorubicin. Molecular & Cellular Biomechanics. 2024; 21: 111. https://doi.org/10.62617/mcb.v21.111

ARTICLE INFO

Received: 20 April 2024
Accepted: 13 June 2024
Available online: 21 June 2024

Abstract: The therapeutic effect of doxorubicin (DOX) on various cancers is enticing, but its huge toxic side effects are equally obvious. Loading it into nanocarriers and then delivering the drug is currently the most promising solution. In this work, we investigate the assembly mechanism of dodecylphosphorylcholine (DPC) aggregates for encapsulating DOXs using molecular dynamics simulation with an all-atomic force field. The principal propellants of the drug encapsulation procedure encompass hydrophobic and van der Waals interactions. Additionally, hydrogen bonding and electrostatic interactions wield significant influence in the aggregation dynamics of DPCs. The radial distribution function indicates that when DPC aggregates act as stable carriers exerting strong adhesion to the drugs, intermolecular interactions predominantly manifest within the spatial interval ranging from 0.5 nm to 1.0 nm. All calculated data and visualized images of the system configuration changing with simulation time reveal that after about 30 ns, the changes in DPC aggregation sites tend to ultimately form multiple aggregates and exhibit a good morphology loaded with DOXs. Our study explored the drug-carrying potential of DPC, which provides an important theoretical basis and effective guidance for researchers to design a more suitable DDS for DOX and then break through the bottleneck of the clinical application of DOX.

Keywords: doxorubicin; dodecylphosphorylcholine; drug delivery system; molecular dynamics simulations; mechanism of drug loading

1. Introduction

Doxorubicin (DOX) stands as a prominent figure among anticancer medications, extensively employed to impede the proliferation and progression of various malignancies, encompassing gastric, pulmonary, mammary, vesical, ovarian, thyroidal, neurogenic, myogenic, articular, and soft tissue carcinomas, among others [1,2]. Its molecular formula is $C_{27}H_{29}NO_{11}$ and its chemical structure is shown in **Figure 1(a_1)**. The therapeutic efficacy of DOX in dismantling the molecular framework of cancer cells and restraining their proliferation frequently coincides with the adverse phenomenon of damaging neighboring healthy cells and impeding their growth [3,4]. Nanotechnology is considered to be the most promising option for attenuating this “negative process” and thus maximizing the drug efficacy of DOX.

This technique is dedicated to the formation of smaller than cell-size particles (drug delivery system, DDS) that can encapsulate the target drug to cross the biological barrier and eventually deliver the drug to the target sites [5–7]. The ideal DDS has excellent biocompatibility, controls and slows drug release mechanisms, protects drug molecules, and increases drug persistence in the bloodstream [8–10].

Matrix materials for DDS mainly include lipids and polymers [11]. In recent years, the molecules of dodecylphosphorylcholine (DPC) have garnered the interest of researchers in the realm of drug design [12–14]. The DPC monomer's molecular formula is $C_{17}H_{38}NO_4P$, with its molecular configuration depicted in **Figure 1(a_2)**. DPC aggregates can exhibit a unique set of advantages as drug carriers. Firstly, as a phospholipid compound, DPC exhibits remarkable biocompatibility due to its similarity to cellular membrane constituents within the body [15,16], thereby aiding in reducing adverse effects on the human body. Secondly, at appropriate concentrations, the surfactant properties of DPC are gentle and do not cause significant disruption to cell membrane structures. By adjusting the concentration, solvent environment, synthesis method and other conditions, the surfactant properties or structure of DPCs can be precisely controlled, such as the characteristic size of their aggregates, which means that their ability to pass through the film and penetrate into biological tissues (mobility and permeability) can be altered, which in turn improves the utilization of the drug. By introducing targeting ligands or modifying functional groups, DPC can achieve targeted drug delivery, thereby enhancing the local therapeutic effects of drugs while minimizing damage to normal tissues. Beyond that, DPC has good solubility and stability for both aqueous and lipid environments [17], and the outer surface of DPC aggregates is difficult to interact with tissue components or blood, which effectively shields the external environment from the drug, and the drug is therefore not easily recognized by phagocytes or specific proteins. This effectively safeguards drug transport and circulation in the body.

Molecular dynamics (MD) serves as a potent instrument for furnishing both qualitative and quantitative insights into the interaction and physicochemical mechanisms inherent in drug systems. Given the considerable expenses associated with experimental testing, numerous investigations presently leverage MD methodologies to simulate DDS. There have been many MD simulation studies involving DOX [18–26]. Some of these recent typical works include: Maleki et al. [24] conducted simulations on the delivery of DOX via N-isopropyl acrylamide (NIP)-carbon nanotube (CNT) composite structures, revealing that 5-mer NIP exhibited superior performance as a carrier for DOX loading compared to 10-mer and 15-mer NIP. Arabian et al. [25] conducted molecular dynamics simulations on carbon nanotubes functionalized with folic acid or tryptophan (FCNTs) for DOX adsorption. The findings indicated a significant increase in FCNTs' solubility in aqueous solutions, with strong interactions observed between drug molecules and FCNTs under physiological pH conditions. Siani et al. [26] provided insights into the penetration and distribution behavior of DOX within the lipid bilayer composed of phosphatidylcholine (PC), sphingomyelin (SM), and cholesterol lipid molecules. However, to our knowledge, DPC aggregates, as a potential DDS for DOX, have limited targeted reports on their self-assembly kinetics in aqueous solutions and their

structural elements for understanding the molecular-level mechanisms of encapsulation and delivery of DOX. And such research is needed because it is a low-cost and effective way to explore novel DDSs adapted to DOX to improve drug efficacy. This paper uses MD simulation to reveal the feasibility of DPCs as DOX delivery carriers, which includes insight into the kinetic mechanism of the aggregation process of DPC molecules, analysis of the interaction between DPC aggregates and drugs, the radius of gyration of aggregates, intermolecular hydrogen bonding, and radial distribution functions, etc., to provide prospective guidance or lay the theoretical foundation for the subsequent experimental synthesis of DDS made of DPCs.

2. Materials and methods

Initially, a cubic simulation box with dimensions of 10 × 10 × 10 nm^3 is assembled. Within this box, three DOX molecules and one hundred DPC molecules are randomly inserted. Subsequently, the system is solvated with water utilizing the SPC model, followed by an energy minimization procedure. The system is then coupled to a temperature of 300 K using the V-rescale algorithm [27] to achieve the NVT ensemble. Next, the Berendsen algorithm [27] is employed to maintain the system pressure at 1.0 atm, stabilizing it to acquire the NPT ensemble. Finally, the completed simulation is conducted over a duration of 60 ns. The entirety of simulations within this study are conducted utilizing the GROMACS package [28,29] and the OPLSAA force field. In addition, covalent bonds including hydrogen atoms reach equilibrium lengths through LINCS algorithm. Employing the particle mesh Ewald [30] summation method to calculate the periodic electrostatic interactions of the entire system. Nonbonded interactions are computed utilizing a dual-cutoff group-based approach, with a r_{cut} of 1.2 nm applied to both electrostatic and Lennard-Jones interactions. The VMD package [31] is employed to generate visual depictions of the molecular configurations within the system. Multiwfn software [32] and VMD software are combined to calculate and visualize the distribution of electrostatic potential on molecular surfaces. They are also used to compute and plot the IGM (Independent Gradient Model) map [33] between molecular components to illustrate the interaction regions, types of interactions, and interaction strengths.

3. Results and discussion

3.1. Visualization analysis of the simulation system

Figure 1 illustrates the aggregation behavior of DPCs and their process of capturing drugs. As shown in **Figure 1a**, at the onset of the simulation, three DOX molecules, depicted as multicolored spheres, and one hundred DPC molecules, represented by multicolored branches, were randomly positioned within the simulation box. After simulating for 20 ns, as shown in **Figure 1b**, DPC molecules exhibit slight local aggregation phenomena, with aggregation sites at random locations not centered on DOXs. When the simulation time is increased to 40 ns, as illustrated in **Figure 1c**, the proximity between DOX molecules diminishes, resulting

in a reduction of dispersion, and it is of interest that the DPC molecules are also highly concentrated and aggregate around the DOXs system at this time. By further extending the simulation time to 60 ns, as shown in **Figure 1d**, the DPC molecules self-assemble to form multiple nearly spherical aggregates, and most of them accumulate at DOX sites to achieve the encapsulation of the target drugs.

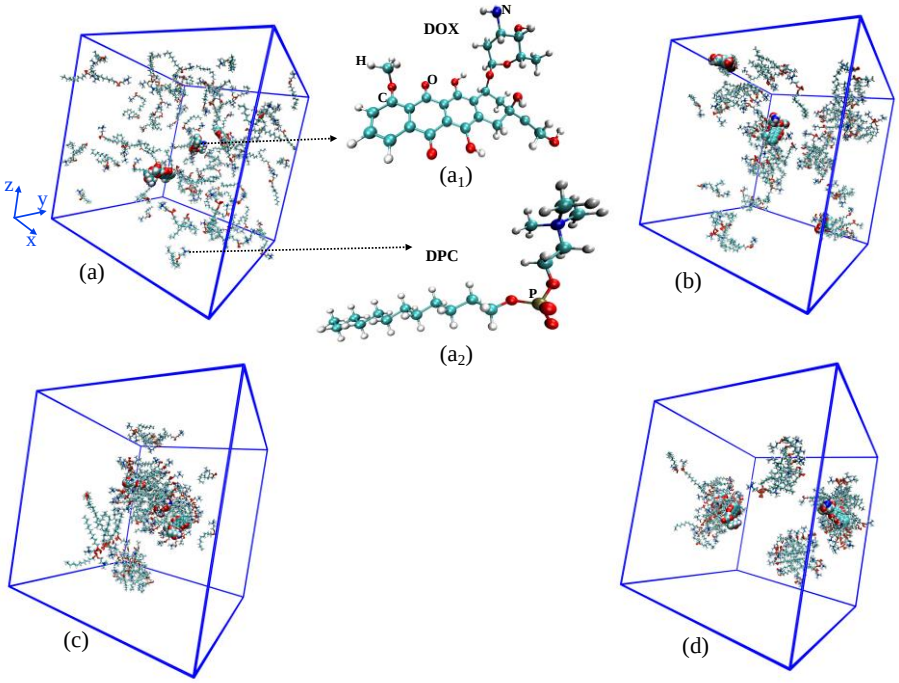

Figure 1. Snapshots are captured at various time points throughout the 60 ns simulation of DPC with DOX: **(a)** at 0 ns; **(b)** at 20 ns; **(c)** at 40 ns; **(d)** at 60 ns.

DPC (sticks), DOX (big spheres). To enhance clarity, water molecules and virtual sites are excluded from the depiction. The insets **(a_1)** and **(a_2)** in **(a)** show the chemical structures of DOX and DPC molecules in three dimensions, respectively.

3.2. Configuration evolution of DPC polymer

To delve deeper into the spatial expansion or density of molecules, we evaluate the gyration radius [34] of the DPC molecular system, which is graphically represented in **Figure 2a**. In this plot, the *x*-axis corresponds to the simulation duration, while the *y*-axis depicts the gyration radius. As seen, the size of the gyration radius fluctuates with time but shows an overall decreasing trend, which indicates a gradual increase in the aggregation of DPC molecules within a region. Combined with **Figure 1**, this (results from **Figure 2a**) implies that the polymer gradually covers the drugs, forming stable complexes.

In **Figure 2b**, the solvent accessible surface area (SASA) for the DPCs ensemble is depicted throughout the simulation. The decrease in SASA values serves as compelling evidence for the transition of molecules from dispersion to aggregation. After the start of the simulation, the SASA value decreases sharply in the first 20 ns as the DPC molecules begin to aggregate, continues to decrease slowly for the next 30 ns, and maintains a relatively stable value in the last 10 ns of the simulation, indicating that the system finally enters into a steady state with the simulation time. The reduction of SASA of aggregates is due to the structural changes of DPC surfactants aggregated in solution preventing the contact of

surfactants with water molecules. The adverse interplay between hydrophobic entities and water represents a significant force fostering the self-assembly of aggregates within aqueous environments. Manifestly, the oscillation observed in the SASA curve portrayed in **Figure 2b** intricately reflects the nuanced shifts in this unfavorable interplay during the aggregation of DPC.

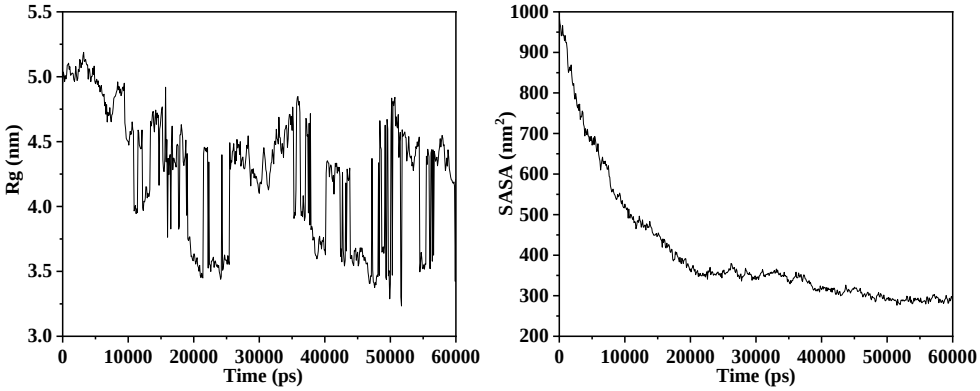

(a) (b)

Figure 2. (a) gyration radius of DPC aggregate over a 60 ns simulation; **(b)** dynamics of the SASAs of the DPC aggregate.

3.3. Interactions between drug, polymer, and solvent molecules

During the 0–60 ns simulation period, averaged amounts of water molecules within a 5 Å range around each DOX molecule are investigated (**Figure 3a**). As shown in the figure, the amount on water molecules around drugs reduces significantly during DPC self-assembly, which means gradual aggregation of DPCs occupies the space of water molecules surrounding drugs and forces these water molecules to be ejected into the bulk solution. This approves more DPC molecules to interact with DOXs, its more visual evidence can also be represented using the number of atom contacts between DOXs and DPCs (**Figure 3b**).

The number of atom contacts [35] formed between DOXs and DPCs can be calculated by the following expression:

$$N_C(t) = \sum_{i=1}^{N_{\mathrm{DPC}}} \sum_{j=1}^{N_{\mathrm{DOX}}} \int_{r_i}^{r_i+0.6\ nm} \delta\big(r(t) - r_j(t)\big)\mathrm{d}r \tag{1}$$

herein, N_{DPC} and N_{DOX} represent the cumulative count of atoms within the molecular assemblies of DPC and DOX, respectively. Meanwhile, r_i signifies the spatial displacement from the *i*-th atom within the DPC ensemble to the *j*-th atom within the DOX configuration. In **Figure 3b**, the illustration depicts the count of atomic contacts occurring involving DOX molecules and DPC polymers. As seen, these counted contacts rise rapidly during the first 20 ns, then increase slowly and remain fluctuating within a range of values, and such fluctuation is attributed to a variation in the DPC aggregation sites, i.e., this is related to the behavior of multiple nanoaggregates aggregating and then dispersing into multiple different groups in **Figure 1**. The evolution of the measured values in **Figure 3a,b** quantitatively demonstrates the progressive intimacy between DOXs and DPCs with increasing simulation time, and the enhanced adhesion between them ensures the stability of

DPC aggregates when used as drug carriers.

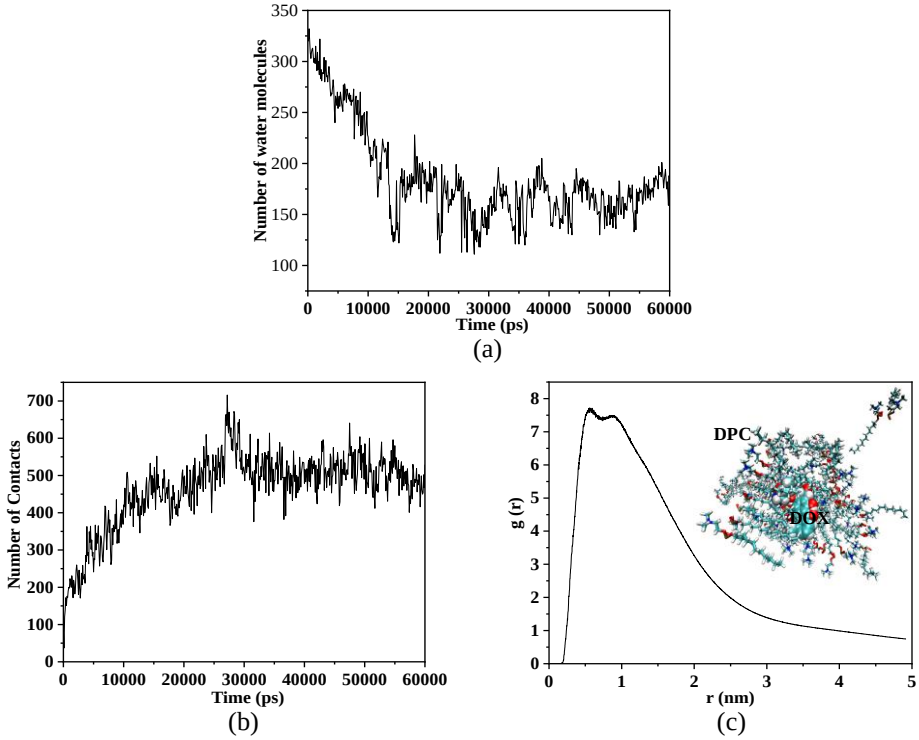

Figure 3. (a) the mean quantity of aqueous molecules surrounding each DOX molecule in the 5 Å range; **(b)** the aggregate tally of contacts involving DOX with DPC; **(c)** RDF among DOX and DPC aggregate.
The illustration in the upper right corner is a snapshot of a DOX molecule and its surrounding environment taken from the 60 ns simulation system.

To gain deeper insights into the environment surrounding DOX molecules, the structural layout of DPC aggregate around DOX molecule is revealed. The radial distribution function (RDF) corresponding to the study system can be calculated using the following equation:

$$g_{\mathrm{DOX-DPC}}(r) = \frac{\langle \rho_{\mathrm{DPC}}(r) \rangle}{\langle \rho_{\mathrm{DPC}} \rangle_{\mathrm{local}}} \frac{1}{\langle \rho_{\mathrm{DPC}} \rangle_{\mathrm{local}}} \frac{1}{N_{\mathrm{DOX}}} \int_{i \in \mathrm{DOX}}^{N_{\mathrm{DOX}}} \int_{j \in \mathrm{DPC}}^{N_{\mathrm{DPC}}} \frac{\delta(r_{ij} - r)}{4\pi r^2} \qquad (2)$$

where $\langle \rho_{\mathrm{DPC}}(r) \rangle$ the partial density of the DPC constituent located r away from the DOX constituent, and $\langle \rho_{\mathrm{DPC}} \rangle_{\mathrm{local}}$ the average partial density of the DPC constituent within all spheres of radius r surrounding all DOX molecules. **Figure 3c** shows the computed results, in which the abscissa is the range from DOX while the longitudinal axis is the RDF $g(r)$. The RDF plot shows a couple of spikes within about 0.5–1.0 nm (the highest of which is close to 0.6 nm), indicating that the interactions between DOXs and DPCs occur mainly in this range. This situation suggests clustering of the DPC surface active agent surrounding the DOX molecule. From this, one can deduce that DOX in wrapped inside the hydrophobic center for DPC aggregate. A typical local snapshot of a system with a simulation time of 60 ns is shown as an attached figure in **Figure 3c**, which can visually help understand the surrounding structure of DOX. It is clear that the conclusions derived from **Figure 3c** are very consistent with the measuring results presented in **Figure 3,b**.

Figure 4a illustrates the fluctuation in the statistical count of hydrogen bonds

[36,37] among DPC and water molecules (DPC-SOL), between DOX and water molecules (DOX-SOL), and between DOX and DPC (DOX-DPC) throughout the simulation. In the figure, the horizontal axis denotes the progression of simulation time, while the vertical axis represents the quantity of hydrogen bonds. Due to the dispersion of DPC molecules throughout the entire environment at the beginning of the simulation, the count of hydrogen bonds linking DPCs and water exhibits an initial high value, gradually diminishing as DPC molecules aggregate and establish bonds amidst themselves. Specifically, as shown in the black curve in **Figure 4a**, the count of hydrogen bonds involving DPCs and water experiences a rapid decline from a notably high level within the initial 20 ns, followed by a gradual decrease over the subsequent 30 ns, and maintains a relatively stable level during the final 10 ns. The temporal evolution depicted aligns with that illustrated in **Figure 2b**, collectively furnishing quantitative evidence supporting the aggregation phenomenon of DPC molecules.

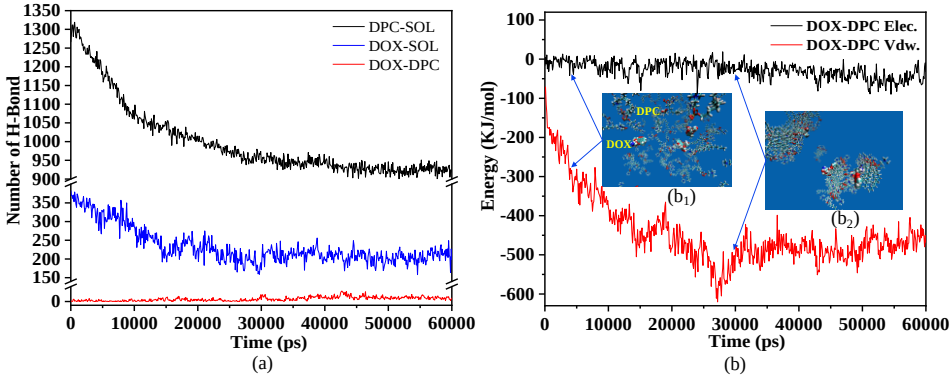

Figure 4. (a) the count of hydrogen bonds among the solvent (SOL), DPC, and DOX; **(b)** the Elec. and Vdw. among DOX with DPC surfactants.
The illustrations **(b_1)** and **(b_2)** in the figure are snapshots of the corresponding system at two different simulation times.

Similarly, the uniform dispersion of DOXs within the aqueous environment contributes to a notable count of hydrogen bonds with water molecules at the onset of the simulation, and as the simulation time increases, DPCs gradually accumulate near DOXs, and this behavior alters the surrounding environment for DOXs, thereby increasing the likelihood that hydrogen bonds form involving DOXs and DPCs. Direct evidence supporting this hypothesis is evident in **Figure 4a**, where the count of hydrogen bonds between DOXs and water steadily decreases over time in the simulation (blue curve), with a concomitant increase in the count of hydrogen bonds of DOXs with DPCs (red curve). This indicates that hydrogen bonding is one of the interactions maintaining the close association between DOXs and DPC molecular clusters, consistent with existing reports on the common occurrence of hydrogen bonding between drug molecules and DDS. For instance, Zhao et al. [37] observe dynamic changes in hydrogen bond formation and dissociation in the Ketoprofen-cyclodextrin system. Zhu and Huang [38], employing DFT calculations, find that the drug fluorouracil is adsorbed within functionalized carbon nanotubes via hydrogen bonds between the F83-H115 and O86-H116 bonds. It is noteworthy that the alterations in the quantity of hydrogen bonds of DOX-SOL and DOX-DPC exhibit a

more gradual trend in contrast to the fluctuations observed in the hydrogen bonds of DPC-SOL. However, the credibility of these observations can be substantiated by considering the limited presence of DOX molecules (only three molecules in the simulated system). Overall, the change in the number of hydrogen bonds in **Figure 4a** demonstrates the overall transformation of the solvent from dispersed to agglomerated.

Providing insight into the interactions is an important way to go to reveal the mechanism of DOXs adsorption on DPC aggregates, and in addition to the hydrogen bonding discussed above, the Lennard-Jones interactions and electrostatic interactions are two other important key components. The Lennard-Jones interaction can be calculated by the following equation:

$$V_{LJ}(r) = 4\varepsilon\left[(\frac{\sigma}{r})^{12} - (\frac{\sigma}{r})^{6}\right] \tag{3}$$

here, r denotes the separation distance between the two particles engaged in interaction, ε represents the potential well's depth, and σ signifies the distance at which the potential energy between the particles is null. The electrostatic interaction consists of Coulomb's formula:

$$|F| = K\frac{|q_1 q_2|}{r^2} \tag{4}$$

here, K represents the Coulomb constant ($K \approx 8.988 \times 10^9\ \mathrm{Nm^2C^{-2}}$), q_1 and q_2 represent charges, while r denotes the separation distance for these two charges. **Figure 4b** exhibits the van der Waals interaction energy (Vdw.) and electrostatic interaction energy (Elec.) between the DOXs and the DPCs. The abscissa represents the simulation time and the longitudinal scale represents the calculated values. Negative energy corresponds to absorbing energy and positivity corresponds to repelling energy. The local snapshots of the system at two typical moments corresponding to the process of interaction changing with simulation time (illustrations **Figure 4(b_1,b_2)**) are shown in this figure.

As depicted in **Figure 4b**, the Vdw. steadily diminish over the course of the simulation, suggesting the adsorption of DOX molecules onto the DPC aggregates. The insets **Figure 4(b_1,b_2)** demonstrate well that this energy change corresponds to the adsorption process. The Vdw. shows a minimum around 27 ns and then rises and remains fluctuating within a certain range, the reason for this fluctuation is similar to the discussion of **Figure 3b** above, i.e., it is related to the variation of the aggregation sites of the DPCs as illustrated in **Figure 1**. Furthermore, during the simulation, the Elec. between the DPCs and DOXs gradually weaken with the adsorption of the drug. Although this change is much more moderate compared to the variations in Vdw., it is still significant enough to demonstrate that electrostatic interactions play a role in the drug encapsulation process.

To further reveal the essence of the intermolecular interactions between DOX and DPC molecules, we calculate the van der Waals surface electrostatic potentials (ESP) of DOX and DPC molecules, which are visualized using isosurfaces colored according to electron density, providing a clear depiction of their surface distributions, and they are displayed in **Figure 5**. In the initial stages of interaction, molecules approach each other through electrostatic attraction. The regions of positive ESP on one molecule tend to contact regions of negative potential on the

other molecule. This tendency is stronger when the positive potential is higher and the negative potential is lower. As shown in **Figure 5**, the regions of negative ESP (blue) and positive ESP (red) in DOX are relatively uniformly distributed. The dodecyl group of the DPC molecule is nearly neutral (white), whereas the phosphoryl and choline groups at the head exhibit distinct regions of surface negative and positive potentials, respectively. This means that at the beginning of the simulation, DPCs are mainly clustered by the proximity of the molecular heads (one end of the choline moiety) to each other or to DOXs, and then the positions of the molecules are continuously adjusted with the change of the relative positions of the molecules in order to minimize the energy of the clusters.

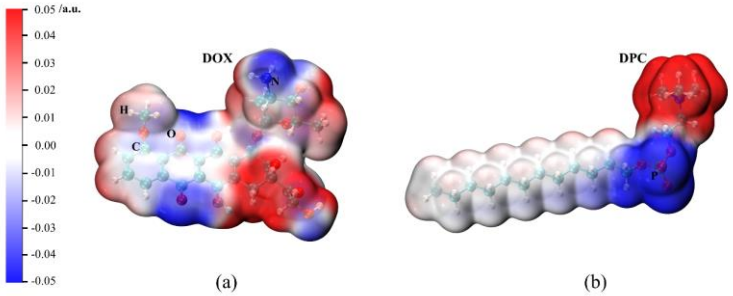

Figure 5. ESP mapped the van der Waals surface of **(a)** DOX; **(b)** DPC molecules.
Significant surface local minima and maxima of the ESP are depicted in blue and red, respectively. The unit is in a.u..

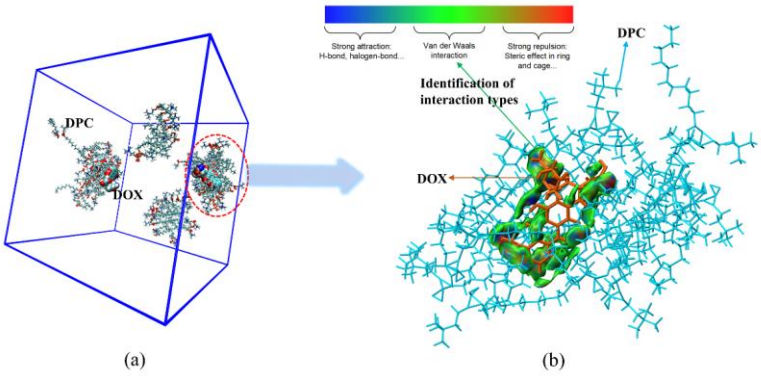

Figure 6. (a) overall configuration of the molecular system under simulation at 60 ns. The portion enclosed by the red dashed line is extracted as the object of interest; **(b)** within the molecular cluster of interest shown in **(a)**, DOX and the system consisting of DPC molecules are defined as two fragments, respectively.
After computation, the IGM map is generated to illustrate the types and regions of interactions between the two segments. For clarity, DOX and DPC are represented by golden and cyan sticks, respectively.

At the end of the simulation (60 ns moment), a region of interest within the resulting system is extracted for detailed analysis, as indicated by the red dashed circle in **Figure 6a**. This extracted region is divided into two segments: segment 1 consisting of DOX molecule and segment 2 containing all DPC molecules. An IGM map [33] is constructed to clearly examine the interaction regions, as well as the types and strengths of interactions between these two segments. The results are presented in **Figure 6b**. In **Figure 6b**, the interaction regions are predominantly green, indicating that the interactions between DOX and DPC molecules are

primarily van der Waals forces. A few green regions show conspicuous blue centers, corresponding to a small number of hydrogen bonds. These findings are consistent with the inferences made in **Figure 4**, collectively emphasizing the predominant role of van der Waals forces in the drug encapsulation process. This aligns with the conclusions drawn by Hasanzade and Raissi [39], who in their research highlighted van der Waals interactions as the primary driving force in DOX drug delivery.

4. Conclusions

In this study, we scrutinize the microstructure for DPC aggregates and the mechanism of DPCs sealing DOXs through MD simulation. During the 60 ns simulation, the gyration radius and SASA of the DPC system gradually diminish with the aggregating of DPCs. During the self-assembly process, DPCs compress the space occupied by water molecules surrounding DOXs, effectively enclosing DOXs within their structure. Consequently, these compressed water molecules are expelled into the bulk solution, resulting in a swift decrease in the statistical count of water molecules around DOXs at the onset of the simulation. Concurrently, there is a rapid increase in the number of atomic contacts between DOXs and DPCs. To become closer of the relationship between DPCs and DOXs also leads to a substantial fall in the number of hydrogen bonds between DPCs and water, as well as between DOXs and water, from their high values when dispersed in solution, while a consequent rise in the number of hydrogen bonds between DPCs and DOXs. Additional scrutiny unveils that DPC aggregates, acting as carriers for drugs, primarily engage with DOX molecules at distances ranging from 0.5 nm to 1.0 nm. The encapsulation of DOXs is predominantly steered by van der Waals interactions, with electrostatic interactions also contributing favorably to the aggregation of DPCs. Moreover, these calculated quantitative data (gyration radius, water molecules around DOXs, atom contacts of DOX-DPC, Vdw., etc.) all fluctuate within a certain numerical range after a simulation time of nearly 30 ns, which is believed to be caused by changes in DPC aggregation sites during their self-organization process. All of the above analyses are consistent with the changes exhibited by the visualization plots of the conformation of the system with simulation time, and evidence for these inferences can be found in these plots in graphic form.

Author contributions: Conceptualization, QS; methodology, QS and ZD; software, ZL; validation, QS and PH; formal analysis, QL; investigation, QL; resources, QS and WW; data curation, ZL; writing—original draft preparation, QS; writing—review and editing, QS and PH; visualization, ZD; supervision, QS; project administration, QS, WW and PH; funding acquisition, QS and QL. All authors have read and agreed to the published version of the manuscript.

Funding: This work was financially supported by the TCM Joint Project of Yunnan Province (No. 202301AZ070001-033 (Q.S.)), Yunnan Science and Technology Talent and Platform Program (No. 202105AG070012MS2301 (Q.S.)), the IUR Innovation Fund of Science and Technology Development Center of the Ministry of Education of China (No. 2021BCA02006 (Q.S.)), Yunnan Provincial Department of Education Science Research Fund (2023J0550 (Q. L.)), the Reserve Talents Project

for Young and Middle-Aged Academic and Technical Leaders of Yunnan Province (No. 202205AC160038 (W.W.)), the National Natural Science Foundation of China (No. 81660665 (W.W.)), the National Natural Science Foundation of China (No. 52161037 (P.H.)), and the National Key Research and Development Program (No. 2021YFB3802400 (P.H.)).

Ethical approval: Not applicable.

Conflict of interest: The authors declare no conflict of interest.

References

1. Wang Q, Jiang F, Zhao C, et al. miR-21-5p prevents doxorubicin-induced cardiomyopathy by downregulating BTG2. Heliyon. 2023; 9(5): e15451. doi: 10.1016/j.heliyon.2023.e15451
2. Abd-Elmoneim OM, Abd El-Rahim AH, Hafiz NA. Evaluation of selenium nanoparticles and doxorubicin effect against hepatocellular carcinoma rat model cytogenetic toxicity and DNA damage. Toxicology Reports. 2018; 5: 771-776. doi: 10.1016/j.toxrep.2018.07.003
3. dos Santos JM, Alfredo TM, Antunes KÁ, et al. Guazuma ulmifolia Lam. Decreases Oxidative Stress in Blood Cells and Prevents Doxorubicin-Induced Cardiotoxicity. Oxidative Medicine and Cellular Longevity. 2018; 2018: 1-16. doi: 10.1155/2018/2935051
4. Jabłońska-Trypuć A, Świderski G, Krętowski R, et al. Newly Synthesized Doxorubicin Complexes with Selected Metals—Synthesis, Structure and Anti-Breast Cancer Activity. Molecules. 2017; 22(7): 1106. doi: 10.3390/molecules22071106
5. Zhang W, Taheri-Ledari R, Ganjali F, et al. Nanoscale bioconjugates: A review of the structural attributes of drug-loaded nanocarrier conjugates for selective cancer therapy. Heliyon. 2022; 8(6): e09577. doi: 10.1016/j.heliyon.2022.e09577
6. Kondiah PPD, Choonara YE, Kondiah PJ, et al. Nanocomposites for therapeutic application in multiple sclerosis. In: Applications of Nanocomposite Materials in Drug Delivery. Woodhead Publishing; 2018; pp. 391-408.
7. Masina N, Choonara YE, Kumar P, et al. A review of the chemical modification techniques of starch. Carbohydrate Polymers. 2017; 157: 1226-1236. doi: 10.1016/j.carbpol.2016.09.094
8. Niu W, Xiao Q, Wang X, et al. A Biomimetic Drug Delivery System by Integrating Grapefruit Extracellular Vesicles and Doxorubicin-Loaded Heparin-Based Nanoparticles for Glioma Therapy. Nano Letters. 2021; 21(3): 1484-1492. doi: 10.1021/acs.nanolett.0c04753
9. Mdlovu NV, Lin KS, Weng MT, et al. Design of doxorubicin encapsulated pH-/thermo-responsive and cationic shell-crosslinked magnetic drug delivery system. Colloids and Surfaces B: Biointerfaces. 2022; 209: 112168. doi: 10.1016/j.colsurfb.2021.112168
10. Darson J, Thirunellai Seshadri R, Katariya K, et al. Design development and optimisation of multifunctional Doxorubicin-loaded Indocynanine Green proniosomal gel derived niosomes for tumour management. Scientific Reports. 2023; 13(1). doi: 10.1038/s41598-023-28891-8
11. Mohanty A, Uthaman S, Park IK. Utilization of Polymer-Lipid Hybrid Nanoparticles for Targeted Anti-Cancer Therapy. Molecules. 2020; 25(19): 4377. doi: 10.3390/molecules25194377
12. Faramarzi S, Bonnett B, Scaggs CA, et al. Molecular Dynamics Simulations as a Tool for Accurate Determination of Surfactant Micelle Properties. Langmuir. 2017; 33(38): 9934-9943. doi: 10.1021/acs.langmuir.7b02666
13. Harris JJ, Pantelopulos GA, Straub JE. Finite-Size Effects and Optimal System Sizes in Simulations of Surfactant Micelle Self-Assembly. The Journal of Physical Chemistry B. 2021; 125(19): 5068-5077. doi: 10.1021/acs.jpcb.1c01186
14. Siebert HC, Eckert T, Bhunia A, et al. Blood pH Analysis in Combination with Molecular Medical Tools in Relation to COVID-19 Symptoms. Biomedicines. 2023; 11(5): 1421. doi: 10.3390/biomedicines11051421
15. Saravanan R, Bhattacharjya S. Oligomeric structure of a cathelicidin antimicrobial peptide in dodecylphosphocholine micelle determined by NMR spectroscopy. Biochimica et Biophysica Acta (BBA)—Biomembranes. 2011; 1808(1): 369-381. doi: 10.1016/j.bbamem.2010.10.001
16. Serra-Batiste M, Ninot-Pedrosa M, Bayoumi M, et al. Aβ42 assembles into specific β-barrel pore-forming oligomers in membrane-mimicking environments. Proceedings of the National Academy of Sciences. 2016; 113(39): 10866-10871. doi: 10.1073/pnas.1605104113

17. Ganapathy S, Opdam L, Hontani Y, et al. Membrane matters: The impact of a nanodisc-bilayer or a detergent microenvironment on the properties of two eubacterial rhodopsins. Biochimica et Biophysica Acta (BBA)—Biomembranes. 2020; 1862(2): 183113. doi: 10.1016/j.bbamem.2019.183113
18. Izadyar A, Farhadian N, Chenarani N. Molecular dynamics simulation of doxorubicin adsorption on a bundle of functionalized CNT. Journal of Biomolecular Structure and Dynamics. 2015; 34(8): 1797-1805. doi: 10.1080/07391102.2015.1092475
19. Mirhosseini MM, Rahmati M, Zargarian SS, et al. Molecular dynamics simulation of functionalized graphene surface for high efficient loading of doxorubicin. Journal of Molecular Structure. 2017; 1141: 441-450. doi: 10.1016/j.molstruc.2017.04.007
20. Karnati KR, Wang Y. Understanding the co-loading and releasing of doxorubicin and paclitaxel using chitosan functionalized single-walled carbon nanotubes by molecular dynamics simulations. Physical Chemistry Chemical Physics. 2018; 20(14): 9389-9400. doi: 10.1039/c8cp00124c
21. Kordzadeh A, Amjad-Iranagh S, Zarif M, et al. Adsorption and encapsulation of the drug doxorubicin on covalent functionalized carbon nanotubes: A scrutinized study by using molecular dynamics simulation and quantum mechanics calculation. Journal of Molecular Graphics and Modelling. 2019; 88: 11-22. doi: 10.1016/j.jmgm.2018.12.009
22. Pakdel M, Raissi H, Shahabi M. Predicting doxorubicin drug delivery by single-walled carbon nanotube through cell membrane in the absence and presence of nicotine molecules: a molecular dynamics simulation study. Journal of Biomolecular Structure and Dynamics. 2019; 38(5): 1488-1498. doi: 10.1080/07391102.2019.1611474
23. Shirazi-Fard S, Mohammadpour F, Zolghadr AR, et al. Encapsulation and Release of Doxorubicin from TiO2Nanotubes: Experiment, Density Functional Theory Calculations, and Molecular Dynamics Simulation. The Journal of Physical Chemistry B. 2021; 125(21): 5549-5558. doi: 10.1021/acs.jpcb.1c02648
24. Maleki R, Afrouzi HH, Hosseini M, et al. Molecular dynamics simulation of Doxorubicin loading with N-isopropyl acrylamide carbon nanotube in a drug delivery system. Computer Methods and Programs in Biomedicine. 2020; 184: 105303. doi: 10.1016/j.cmpb.2019.105303
25. Arabian T, Amjad-Iranagh S, Halladj R. Molecular dynamics simulation study of doxorubicin adsorption on functionalized carbon nanotubes with folic acid and tryptophan. Scientific Reports. 2021; 11(1). doi: 10.1038/s41598-021-03619-8
26. Siani P, Donadoni E, Ferraro L, et al. Molecular dynamics simulations of doxorubicin in sphingomyelin-based lipid membranes. Biochimica et Biophysica Acta (BBA)—Biomembranes. 2022; 1864(1): 183763. doi: 10.1016/j.bbamem.2021.183763
27. Ke Q, Gong X, Liao S, et al. Effects of thermostats/barostats on physical properties of liquids by molecular dynamics simulations. Journal of Molecular Liquids. 2022; 365: 120116. doi: 10.1016/j.molliq.2022.120116
28. Van Der Spoel D, Lindahl E, Hess B, et al. GROMACS: Fast, flexible, and free. Journal of Computational Chemistry. 2005; 26(16): 1701-1718. doi: 10.1002/jcc.20291
29. Kutzner C, Kniep C, Cherian A, et al. GROMACS in the Cloud: A Global Supercomputer to Speed Up Alchemical Drug Design. Journal of Chemical Information and Modeling. 2022; 62(7): 1691-1711. doi: 10.1021/acs.jcim.2c00044
30. Darden T, York D, Pedersen L. Particle mesh Ewald: An N · log(N) method for Ewald sums in large systems. The Journal of Chemical Physics. 1993; 98(12): 10089-10092. doi: 10.1063/1.464397
31. Humphrey W, Dalke A, Schulten K. VMD: Visual molecular dynamics. Journal of Molecular Graphics. 1996; 14(1): 33-38.
32. Lu T, Chen F. Multiwfn: A multifunctional wavefunction analyzer. Journal of Computational Chemistry. 2011; 33(5): 580-592. doi: 10.1002/jcc.22885
33. Lefebvre C, Rubez G, Khartabil H, et al. Accurately extracting the signature of intermolecular interactions present in the NCI plot of the reduced density gradient versus electron density. Physical Chemistry Chemical Physics. 2017; 19(27): 17928-17936. doi: 10.1039/c7cp02110k
34. Zhu Y, Wang J, Vanga SK, et al. Visualizing structural changes of egg avidin to thermal and electric field stresses by molecular dynamics simulation. LWT. 2021; 151: 112139. doi: 10.1016/j.lwt.2021.112139
35. Sica MP, Kortsarz MV, Morillas AA, et al. Protocol to study the oligomeric organization of single-span transmembrane peptides using molecular dynamics simulations. STAR Protocols. 2022; 3(3): 101636. doi: 10.1016/j.xpro.2022.101636
36. Abdulkareem U, Kartha TR, Madhurima V. Radial distribution and hydrogen bonded network graphs of alcohol-aniline binary mixture. Journal of Molecular Modeling. 2023; 29(5). doi: 10.1007/s00894-023-05558-9
37. Zhao Q, Gao H, Su Y, et al. Experimental characterization and molecular dynamic simulation of ketoprofen-cyclodextrin

complexes. Chemical Physics Letters. 2019; 736: 136802. doi: 10.1016/j.cplett.2019.136802

38. Zhu X, Huang Y. Theoretical study on paramagnetic amino carbon nanotube as fluorouracil drug delivery system. Journal of Drug Delivery Science and Technology. 2022; 75: 103670. doi: 10.1016/j.jddst.2022.103670
39. Hasanzade Z, Raissi H. Molecular mechanism for the encapsulation of the doxorubicin in the cucurbit[n]urils cavity and the effects of diameter, protonation on loading and releasing of the anticancer drug: Mixed quantum mechanical/ molecular dynamics simulations. Computer Methods and Programs in Biomedicine. 2020; 196: 105563. doi: 10.1016/j.cmpb.2020.105563